Journal of Solid State Chemistry 183 (2010) 2261–2267

Contents lists available at ScienceDirect

Journal of Solid State Chemistry

journal homepage: www.elsevier.com/locate/jssc

Predicted energies and structures of β–$Ca_3(PO_4)_2$

E.E. Jay [a], E.M. Michie [a], D. Parfitt [a], M.J.D. Rushton [a], S.K. Fong [b], P.M. Mallinson [b], B.L. Metcalfe [b], R.W. Grimes [a,*]

[a] Department of Materials, Imperial College London, London SW7 2AZ, UK
[b] Materials Science Department, AWE, Aldermaston, Berkshire RG7 4PR, UK

ARTICLE INFO

Article history:
Received 11 March 2010
Received in revised form
27 July 2010
Accepted 8 August 2010
Available online 17 August 2010

Keywords:
Whitlockite
β-$Ca_3(PO_4)_2$
Radioactive wasteforms
Space group

ABSTRACT

One of the 6*a* cation sites of the β-$Ca_3(PO_4)_2$ structure has previously been described as half occupied. Here, classical static lattice techniques are used to model the different configurations that the Ca ions can exhibit over these Ca(4) 6*a* sites. All possible configurations in the single primitive unit cell and a hexagonal supercell $3_h \times 1 \times 1$ have been generated, along with configurationally averaged structures, that exhibit the experimentally reported *R* 3*c* symmetry. The lowest energy configuration of the primitive cell exhibits *R* 3 symmetry. Conversely, the lowest energy configurations derived from the hexagonal supercell, which are considerably more stable, exhibit *P* 3_1 and *P* 3_2 symmetries, which are isomorphic supergroups of *R* 3*c*. The implication of these simulations are discussed in terms of refined structural models of the material.

1. Introduction

1.1. Motivation

The family of tricalcium phosphates (also known as calcium orthophosphates) are observed in a wide range of circumstances, from biological systems such as dental calculi, to lunar materials and asteroids [1]. They are also used in applications such as Ca–Ni phosphates in catalysis [2] and fertilizers [3]. As bioactive materials they can combine directly with hard tissues without fibrous connective tissues and are therefore used in applications such as bone fillers and artificial tooth roots [4].

Calcium phosphate minerals are also being considered as alternative materials for radioactive waste forms. The structure provides considerable compositional flexibility and substantial non-stoichiometry, ideal for incorporating a range of waste species. Previous studies have investigated the incorporation of lanthanides including gadolinium and thorium [5,6]. It has also been suggested that tricalcium phosphate is resistant to radiation damage [7], an obviously favourable property for a waste form.

When considering the specific applications mentioned above, it is important to understand the intrinsic and extrinsic defect processes that control the compositional variation. This would be aided by an improved understanding of the basic β–$Ca_3(PO_4)_2$ structure.

Tricalcium phosphate exhibits two polytypes, α–tricalcium phosphate and β–tricalcium phosphate. β–$Ca_3(PO_4)_2$ is stable below 1120 °C, whereas α–$Ca_3(PO_4)_2$ is the high temperature phase, stable between 1120 and 1470 °C [8]. α–$Ca_3(PO_4)_2$ is monoclinic, and exhibits space group *P* 21/*a* [9]. Addition of Mg has been shown to stabilise the β–$Ca_3(PO_4)_2$ structure above 1120 °C [10]. This study will consider β–$Ca_3(PO_4)_2$ which is typically synthesised via the solid-state reaction between $CaHPO_4$ and $CaCO_3$ [11–13]. There is often confusion between different compositions of tricalcium phosphate minerals. The mineral Whitlockite, is closely related, exhibiting similar crystallography to β–$Ca_3(PO_4)_2$ but incorporates not only Ca but also Mg and H [14] and is therefore distinct from β–$Ca_3(PO_4)_2$.

1.2. Description of structure

β–$Ca_3(PO_4)_2$ is traditionally reported as rhombohedral with space group *R* 3*c* [10]. There are five non-equivalent cation sites, three 18*b* and two 6*a* sites, with one site, Ca(4), assigned as half occupied. The structure can be broken down into two columns, A and B, each composed of CaO_n and PO_4 groups, in chains, along the [0001] direction (i.e. parallel to the *c*-axis). As depicted in Fig. 1 and corresponding to Table 1, column A is made up of $P(1)O_4$–$Ca(4)O_3$–$Ca(5)O_6$–$P(1)O_4$–$Ca(4)O_3$–$Ca(5)O_6$–$P(1)O_4$, while column B is made up of $Ca(2)O_8$–$P(2)O_4$–$P(3)O_4$–$Ca(1)O_7$–$Ca(3)O_8$–$Ca(2)O_8$–$P(2)O_4$–$P(3)O_4$–$Ca(1)O_7$–$Ca(3)O_8$. Therefore, only A columns contain Ca(4) sites.

β–$Ca_3(PO_4)_2$ has a unit cell containing 21 formula units of $Ca_3(PO_4)_2$ of dimension: $a \equiv b = 10.4352$ Å, $c = 37.4029$ Å [11]. The

* Corresponding author.
E-mail address: r.grimes@ic.ac.uk (R.W. Grimes).

0022-4596/$ - see front matter Crown Copyright © 2010 Published by Elsevier Inc. All rights reserved.
doi:10.1016/j.jssc.2010.08.008

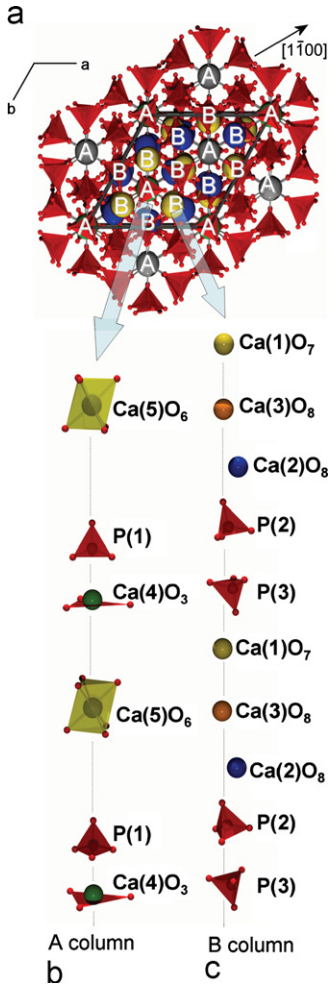

Fig. 1. (a) The β–$Ca_3(PO_4)_2$ structure viewed along [0001], indicating the A and B columns; (b and c) illustrate the configurations of CaO_n and PO_4 groups in the A and B columns.

Table 1
Occupancy of the different sites of β–$Ca_3(PO_4)_2$ as reported by Yashima et al. [11].

Ion	Coordination	Site	Occupancy[a]	Occupancy[a]	B (Å^2)
Ca(1)	CaO_7	18*b*	0.96	1.0	0.38
Ca(2)	CaO_8	18*b*	1.02	1.0	0.27
Ca(3)	CaO_8	18*b*	0.92	1.0	0.76[a]
Ca(4)	CaO_3	6*a*	0.36	0.43	2.0
Ca(5)	CaO_6	6*a*	1.11	1.0	0.76[a]

(a) a preliminary refinement and (b) a final refinement—see text for details. B are the isotropic thermal parameters reported for each site.

[a] Thermal parameters were constrained to be equal.

experimentally derived occupancies and the isotropic thermal parameters (B) are displayed in Table 1. Two refinements are presented (as previously reported [11]): a preliminary refinement (a), where the occupancies of the five sites were allowed to vary freely whilst the isotropic thermal parameters were fixed to be equivalent for all sites, and a final refinement (b), where the occupancies of Ca(1), Ca(2), Ca(3) and Ca(5) were set equal to 1 and the isotropic thermal parameters were allowed to vary along with the occupancy of the Ca(4) site. For refinement (b) the isotropic thermal parameters for the Ca(3) and Ca(5) sites were constrained to be equal. We note that both refinements give rise to significantly non-stoichiometric compositions and that Yashima et al. restricted the thermal parameters to be isotropic because of convergence difficulties if anisotropic thermal parameters were allowed.

1.3. Half occupancy of the Ca(4) site

The neutron diffraction study of Yashima et al. [11] suggests a partial occupancy of the Ca(4) site. It is of interest, and of great importance for the defect chemistry, to assess how the partial occupancy occurs. β–$Ca_3(PO_4)_2$ is not a Ca ion conductor and therefore the disorder is unlikely to be a dynamic mechanism in which the Ca(4) site is occupied by passing Ca ions. The remaining possibilities are therefore; (i) the Ca(4) sites are randomly occupied (i.e. the probability of finding a Ca atom at a site is independent of the occupancy of adjacent sites) (ii) the observed partial occupancy is a symptom of a lower symmetry supercell structure, or (iii) there is local order, so that the probability of finding a Ca atom does not depend upon the occupancy of adjacent sites but this does not extend to complete long range order.

1.3.1. Single unit cell ($1 \times 1 \times 1$)

Considering half occupancy of the 6*a* site Ca(4), it is apparent that for a single unit cell there are three fundamentally different ways for the ions to occupy the six possible Ca(4) sites within each unit cell. These distinct arrangements of the lattice are most easily described in terms of packing or occupancy of the Ca(4) site in A columns. In each A column there are two Ca(4) sites in each of the A columns. Per unit cell, however, they are in a staggered arrangement with respect to each other, as illustrated by Fig. 2 (a–c). So, any column can either have both sites occupied (F), one site occupied and the other vacant (H), or both the Ca(4) sites vacant (E), leading to three basic arrangements. To maintain stoichiometry they have to be arranged such that in total half of the 6 Ca(4) sites are occupied.

The first arrangement, in which the occupied Ca(4) sites are in closest proximity to each other, is illustrated in Fig. 2(a). The Ca(4) sites are occupied alternately down each A column (H, H, H), parallel to the c-axis. As such, along the direction of Ca(4) sites diagonally across the cell, there will be three sites occupied in a row, followed by three vacant sites. There are six possible configurations with this arrangement. Fig. 2(b) shows a second arrangement in which the columns are filled both alternately down the c-axis (H) but in this case alternately across the columns. To distinguish arrangement 4(b) from 4(a) we note that the Ca(4) occupancy of the second half filled column is inverted and so is described as H' producing an H, H', H pattern. This arrangement gives the greatest distance between Ca ions. There are two possible arrangements of this configuration corresponding to H, H', H and H', H, H' (note: although these have the same energy and there are only two distinct configurations in a $(1 \times 1 \times 1)$ cell, as we shall see later in a larger cell this is not necessarily so). The remaining possible arrangement of ions, shown in Fig. 2(c), has one column fully occupied (down the c-axis) (F), one adjacent column where all Ca(4) sites in that column are vacant (E) while the remaining column is half occupied (H). There are 12 possible arrangements of this configuration. In total there are twenty configurations, which corresponds to the expected 6!/3!3! possible ways of arranging three species over six sites. Of course, since we are considering a periodic system, many of these will be symmetrically equivalent and will therefore have the same energy.

When predicting differences between the three types of occupancy arrangement, it seems likely that the relative distances between occupied Ca(4) sites will have a significant effect on the

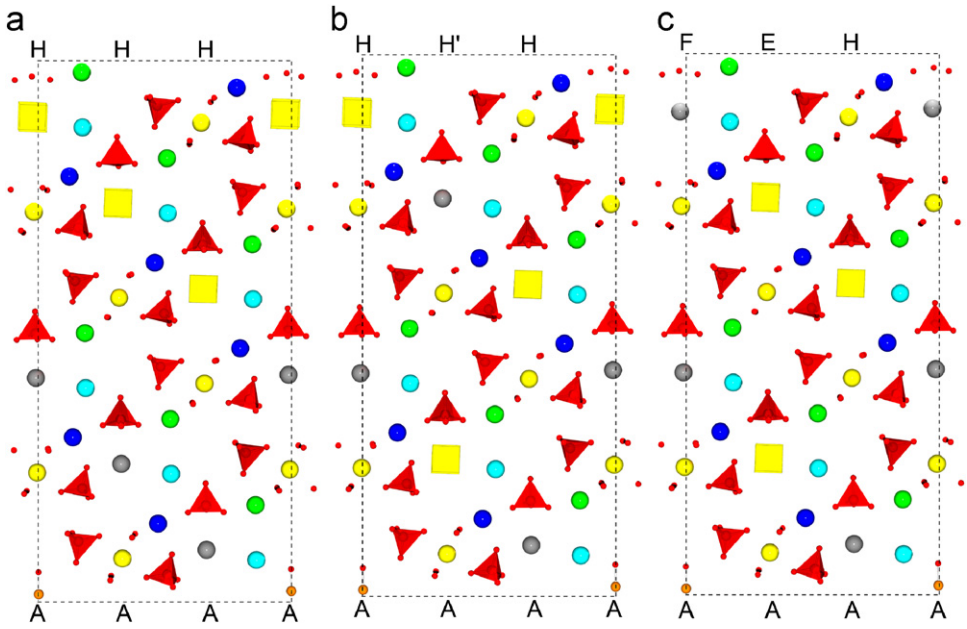

Fig. 2. A series of schematics illustrating the three basic arrangements of half occupying site Ca(4) over the A columns. Where the dashed line outlines a unit cell along the $(1\bar{1}20)$ plane. Vacant Ca(4) sites are represented by a yellow box and occupied sites are grey. The remaining cation sites Ca(1), (2), (3) and (5) are coloured green, blue, cyan and yellow, respectively. The phosphate groups are depicted as red tetrahedra. Note: H' HH' $\equiv$ HH' H in a $(1 \times 1 \times 1)$ cell. (a) The Ca(4) sites are occupied alternately down the A columns, parallel to the *c*-axis and each "adjacent" Ca(4) site across the A columns is occupied; (b) the Ca(4) sites are occupied alternately down the A columns, parallel to the *c*-axis and across the columns; (c) the Ca(4) sites are fully occupied down one A column, with one adjacent A column empty (i.e all possible Ca(4) sites in that column are vacant) and the remaining A column is half occupied, alternating the occupancy parallel to the *c*-axis. (For interpretation of the references to color in this figure legend, the reader is referred to the web version of this article.)

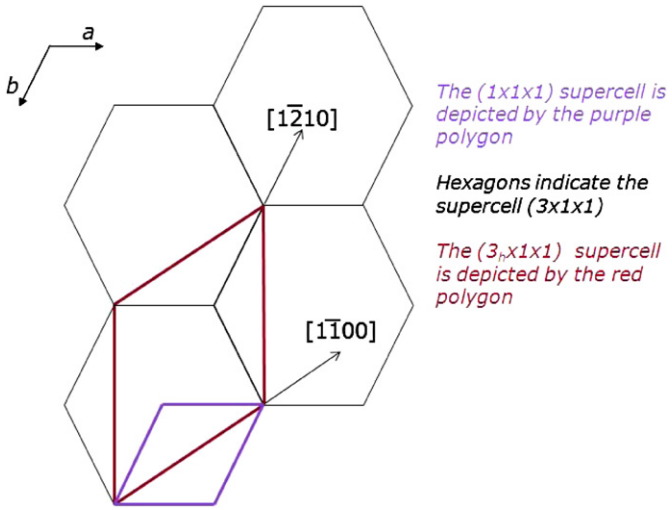

Fig. 3. Polygons representing the different possible basal planes for different cell sizes of β–$Ca_3(PO_4)_2$.

relative lattice energies. Ca(4) sites occupied in closer proximity to each other might demonstrate a greater Coulombic repulsion, leading to a less favourable configuration. However, lattice relaxations associated with and allowed by specific configurations may alter this view.

1.3.2. Full hexagonal cell $(3_h \times 1 \times 1)$

Larger cell sizes will allow for a far greater number of possible configurations, Fig. 3 illustrates the different cell sizes and their respective basal planes. Each $(3_h \times 1 \times 1)$ supercell contains eighteen Ca(4) (6*a*) sites. There are, therefore, a total of 48,620 possible configurations, which equivalent to the single unit cell, corresponds to 18!/9!9! different ways of arranging nine ions over the eighteen Ca(4) sites. As before, many will be symmetrically equivalent and have identical lattice energies. Unlike the single unit cell, however, it is not as clear how to group the many configurations in terms of the proximity of occupied Ca(4) sites. The most stable configuration are therefore identified only in terms of the full (*F*), half occupied (*H*) and empty (*E*) A columns.

1.4. Atomic scale simulations

All structures of β–$Ca_3(PO_4)_2$ were modelled using a classical static lattice technique, which is based on interatomic potentials. This work employed the computer code GULP [15] to calculate the total lattice energies of structures subject to energy minimisation via the BFGS algorithm [16] under constant pressure conditions. This allows the lattice parameters to relax to zero strain and ion positions to move towards the minimum lattice energy for a specific configuration. The Buckingham potential was used to describe the short range interaction energy, between two ions *i* and *j* separated by a distance r_{ij}:

$$\Phi_{ij}(r_{ij}) = A_{ij}\exp\left(\frac{-r_{ij}}{\rho_{ij}}\right) - \frac{C_{ij}}{r_{ij}^6} \quad (1)$$

where, A_{ij}, $\rho_{i,j}$, and C_{ij}, are adjustable parameters. For β–$Ca_3(PO_4)_2$ the potentials act between two pairs of *O* ions and between *O* and Ca ions. In each case the short-range cut-off used was 13 Å. Long-range coulomb forces act between all pairs of ions except those within the same PO_4 tetraherdon. Coulomb interactions are summed using the Ewald technique [17]. In conjunction with the Buckingham potential, a Morse potential (Eq. (2), where *i* and *j* are *P* and *O* ions) and a three body potential (Eq. (3), where *i*, *j* and *k* are *O*, *P* and *O*, respectively) was also used to describe the

Table 2
Potential parameters for β–$Ca_3(PO_4)_2$ [18].

Ion-pair	A (eV)	ρ (Å)	C (eV Å^6)
Buckingham potential			
Ca_{core}–O_{shell}	1550	0.297	0
O–O	16372	0.213	3.47
Morse potential			
	D (eV)	α (Å^{-1})	r_0 (Å)
P–O_{core}	3.47	2.03	1.6
Three body potential			
	k (eV rad^{-2})	Θ (deg)	
O_{core}–P–O_{core}	1.322626	109.47	
Ion	Charge		Core–shell interactions
	Core	Shell	k (eV Å^{-2})
Ca	2		
P	1.18		
O	0.587	−1.632	507.4

intra-ionic interactions governing the phosphate tetrahedra.

$$\Phi_{i,j}(r_{ij}) = D_{i,j}(1-e^{-\alpha(r_{i,j}-r_0)})^2 - D_{i,j} \quad (2)$$

$$\Phi_{i,j,k}(r_{i,j,k}) = \tfrac{1}{2}k_{i,j,k}(\theta_{i,j,k}-\theta_0)^2 \quad (3)$$

The perfect lattice is simulated by defining a unit cell of ions that is repeated throughout space according to periodic conditions. Allowing the ions and lattice vectors of the unit cell to relax to zero strain, minimizes the total lattice energy. The model parameters used in this work were derived by Mkhonto and de Leeuw [18] for the apatite structure and are reported in Table 2.

1.5. Selection of half occupancy configurations

For the simulations of a single unit cell of β–$Ca_3(PO_4)_2$, calculations were carried out in which half of the Ca(4) 6*a* sites were occupied by Ca ions [10,11], for all twenty of the possible $(1\times1\times1)$ configurations described earlier. In addition, a configuration in which all six of the Ca(4) sites were half occupied was simulated, by applying mean field theory [15]. In this case each Ca(4) site has the mean potential of all the possible configurations. This provides the base calculation against which all other calculations are compared. For the $(3_h\times1\times1)$ cell all 48,620 different possible configurations were simulated.

In the neutron diffraction data of Yashima et al., the occupancy and thermal parameters of the Ca(5) sites was regarded as very strongly correlated with other refinement parameters: for example, it was necessary to constrain the thermal parameter to be equal to the value of the Ca(3) site to prevent it adopting un-physical values. We have therefore, investigated a further twenty configurations in which we examine partial occupancy of the Ca(5) sites. This allows us to investigate whether the observed partial occupancy of the Ca(4) sites is actually either part or wholly linked to disorder on the Ca(5) sites.

1.6. Configurational averaging

A statistical thermodynamic average over the symmetry distinct configurations generated for a specific cell size, can be used to generate particular property values [19,20]. If configuration i has property value P_i (here, these will include lattice parameters, unit cell volumes and lattice energies), then the configurational average, $\langle P\rangle$, is given by Eq. (4):

$$\langle P\rangle = \frac{\sum n_i P_i e^{-\Delta E_i/k_B T}}{\sum n_i e^{-\Delta E_i/k_B T}} = \sum C_i P_i \quad (4)$$

where, ΔE_i is the difference between the energy of configuration i and the energy of the most stable configuration, k_B is Boltzmann's constant, T is the temperature over which the average is taken, n_i is the number of equivalent configurations that can be generated in the unit cell and C_i are coefficients that describe the relative contribution of configuration i to the configurational average.

2. Results and discussion

2.1. Single unit cell $(1\times1\times1)$

Using the relaxed positions of the ions from the mean field structure, calculations were carried out occupying the Ca(4) sites as per the twenty different configurations. The results, presented in Fig. 4, show that this gives rise to three energetically distinct structures. This follows the structural description earlier (Fig. 2) where the three main arrangements lead to different spatial separations of the Ca(4) sites. The most stable structure (i.e. that with the lowest lattice energy) corresponds to the situation where Ca(4) atoms have the greatest possible separation (henceforth these will be referred to as, LECs, the Lowest Energy Configurations), as shown in Fig. 2(b). This is in agreement with a previous density functional study by Yin et al. [21] which suggested that the distributions of the Ca(4) ions in the β–$Ca_3(PO_4)_2$ structure affects the stability and electronic properties and of those configurations investigated, the structure with uniformly distributed Ca vacancies was the most stable (however, all configurations were not investigated by Yin et al. [21]).

For the 12 intermediate arrangements (IECs or Intermediate Energy Configurations) illustrated in Fig. 2(c), since the Ca(4) sites are closer together, the lattice energy is higher (but all 12 are identical). For the six configurations that exhibit occupied Ca(4)

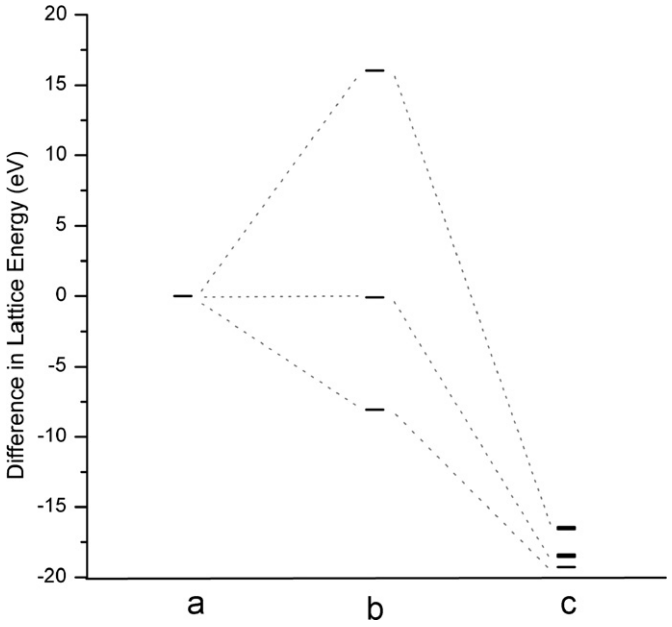

Fig. 4. A comparison of lattice energies for the structure of β–$Ca_3(PO_4)_2$ generated by different simulations: (a) is a mean field calculation in which lattice vectors and ion position have been allowed to relax under a process of energy minimization. This also provides the zero of energy and (b) are calculations for all configurations, using the mean field positions found in (a) and (c) are the same configurations but after full relaxation.

sites closest together (HECs or Highest Energy Configurations) shown in Fig. 2(a), the lattice energy is highest. Fig. 4(b) illustrates this splitting of the "unrelaxed" lattice energies. The space group $P\ 3$ was determined for each of the configurations using the unrelaxed mean field positions, except for the most stable LEC structure, which was found to exhibit $R\ 3$.

Optimising or relaxing the structures of the different configurations both lowers their lattice energy and reduces the variance in energy between the different structures, (illustrated in Fig. 4(c)). The LECs remain the most energetically favourable structure, again with a space group R3c. In this case both configurations have the same fully relaxed energy and are symmetrically identical (in Eq. (4) the value of n_i for this configuration is therefore equal to 2). Post relaxation, the IEC and HEC configurations now exhibit space group P1. It is clearly crucial to carry out a full relaxation in order to derive appropriate results. Now that the ordered structures and in particular the lowest energy structure have been identified, it is necessary to make comparison with average structures (that were previously thought to be closer to experimental data). Average structures can be based on mean field or configurational average models.

In applying mean field theory it is assumed that all configurations are equally likely. This is possible for materials where there is little energetic difference between configurations or where formation kinetics dominate over thermodynamics, so that the structures do not approach a Boltzmann's distribution. Fig. 4, however, demonstrates that there is a significant energetic difference between configurations. Indeed, a configurational average (taken at a temperature of 1000 K) of the different structures shows the LECs are by far dominant (the C_i is 0.9995). This is why the LEC and configurational average results shown in Table 3 are the same.

Overall, the results reported in Table 3 show that all $(1\times1\times1)$ based models slightly underestimate the a and b lattice parameters, leading to a unit cell approximately 3% smaller than reported experimentally. The c/a ratio is also close to the ratio of the experimentally derived parameters, this time approximately 3% larger. Unfortunately the similarity of the mean field and configurational average predictions, makes it clear that comparison of structural parameters will not allow us to differentiate between these models. Nevertheless, the dominance of the LEC even at 1000 K (i.e. not at low temperature) is not consistent with an average occupancy model.

The $(1\times1\times1)$ simulations were repeated with the Ca(5) site half occupied instead of the Ca(4) site and all possible configurations calculated. It was found that the lattice energy for the most stable half occupied Ca(5) site configuration was 0.17 eV per formula unit less stable than the least stable Ca(4) configuration i.e. than the HEC structure. This is consistent with the Ca(4) being half occupied, not Ca(5), in agreement with experiment.

Table 3
A comparison of experimental [11], $(1\times1\times1)$ (LEC) and $(3_h\times1\times1)$ simulated structures.

Cell parameters	Space group	a (Å)	b (Å)	c (Å)	α (deg)	β (deg)	γ (deg)	Volume (Å^3)	c/a ratio
Experimental	$R\ 3c$	10.44	10.44	37.40	90.00	90.00	120.00	3527.26	3.58
Mean field (relaxed)	$R\ 3$	10.29	10.29	37.26	90.00	90.00	120.00	3416.36	3.62
$(1\times1\times1)$ Config. av. at 1000 K	$R\ 3c$	10.28	10.28	37.46	89.99	90.00	120.00	3428.76	3.64
$(1\times1\times1)$ LEC	$R\ 3$	10.28	10.28	37.39	90.00	90.00	120.00	3423.86	3.64
Lowest $(3_h\times1\times1)$	$P\ 3_1$	10.43	10.43	37.40	90.00	90.00	120.00	3527.13	3.59
$(3_h\times1\times1)$ Config. av. at 1000 K	$P\ 3_1$	10.28	10.29	37.37	89.99	90.01	120.00	3421.40	3.63

The relaxed mean field, configurational average and cell parameters for β–$Ca_3(PO_4)_2$ are compared. Due to the increased cell parameters, the results for the $(3_h\times1\times1)$ cells, have been altered for ease of comparison; the lattice energy and cell volume have been divided by 3 and the a and b lattice parameters have been divided by $\frac{\sqrt{3}}{3}$.

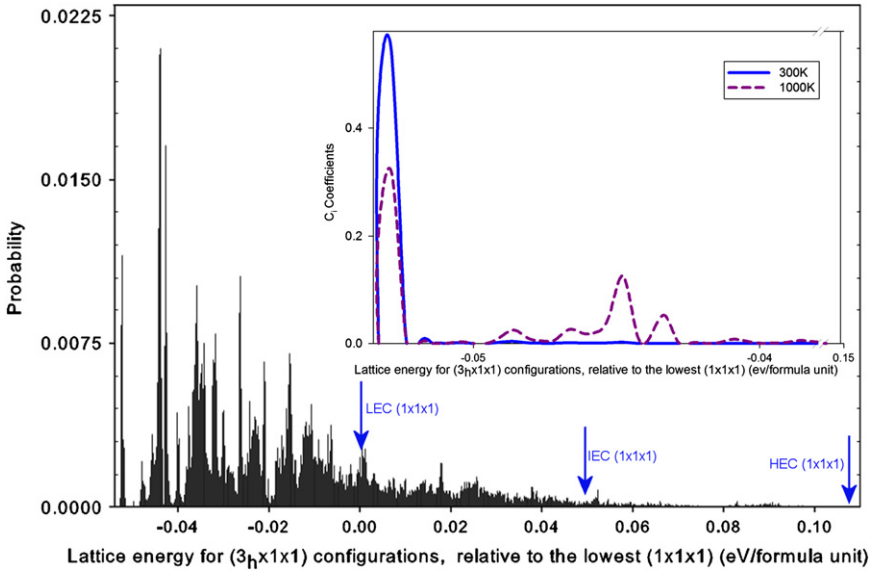

Fig. 5. A histogram to illustrate (a) the number of configurations of half occupied Ca(4) sites in β–$Ca_3(PO_4)_2$, relaxing to a given lattice energy, for the full hexagonal cell, $(3_h\times1\times1)$ relative to the lowest energy single unit cell $(1\times1\times1)$ configuration at 0.0 eV, bin width of 0.01 (eV) and (b) shows the probability of the structure occupying any given state as indicated by the lattice energy per formula unit at 300 and 1000 K.

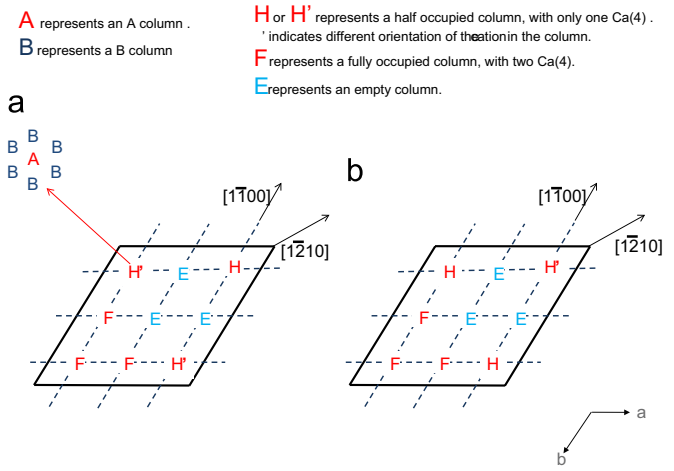

Fig. 6. A schematic of the lowest energy configuration generated within the $(3h \times 1 \times 1)$ cell. Each intersection of the dotted lines represents an A column which is surrounded by six B columns. The occupancy of the columns by Ca(4) is represented by H for half full (1 Ca(4)), *F* for Full(2 Ca(4)) and no change indicates A columns empty of Ca(4): (a) represents one of the two lowest energy configurations attained, with a symmetry of *P* 3_1 and (b) represents the other low energy configuration which has a symmetry of *P* 3_2. Both the low energy configurations have symmetries which are isomorphic supergroups of the unit cell symmetry *R* 3*c*.

2.2. Full hexagonal cell $(3_h \times 1 \times 1)$

Over half of the 48,620 different possible configurations within the $(3_h \times 1 \times 1)$ cell were found to have lower lattice energies than the LEC structure of the $(1 \times 1 \times 1)$ unit cell. Fig. 5 displays a histogram comparing the distribution of lattice energies for the different configurations generated within both cell sizes [11].

The distribution of the occupied Ca(4) sites in the two most stable configuration of the $(3_h \times 1 \times 1)$ cell are illustrated in Fig. 6. Considering the first most stable configuration, in viewing down the *c* axis a longer range ordering of half, full and vacant columns is evident. There are three columns that have a full compliment of Ca ions occupying the Ca(4) sites (*F*), three columns that are half occupied (*H* or *H*′) and three columns that are unoccupied (*E*). The same is true of the second most stable configuration (with only a subtle change in order of *E* and *F* columns around *H* or *H*′ to differentiate these patterns). Nevertheless, the larger cell provides for an enormous number of different *E*, *F*, *H* and *H*′ configurations that are only slightly different and therefore of similar energy.

If we consider the LEC $(1 \times 1 \times 1)$ cell, the three columns arranged in the [1$\bar{1}$00] direction were all half occupied (*H*). In the $(3_h \times 1 \times 1)$ cell there are three sets of three columns along [1$\bar{1}$00] each with a different combination of *F*, *H*, (or *H*′) and E columns. However, if we consider three sets of three columns along [1$\bar{2}$10], the pattern of *F*, *E*, *H* is repeated. This suggests that the lowest energy arrangements of the $(3_h \times 1 \times 1)$ cell have symmetries that can be related back to the original $(1 \times 1 \times 1)$ LEC cell as symmetry sub-groups. The $(1 \times 1 \times 1)$ LEC has a symmetry R3c; the two lowest energy $(3_h \times 1 \times 1)$ configurations have symmetries *P* 3_1 and *P* 3_2, both of which are minimal isomorphic subgroups of *R* 3*c* and are yet to be observed.

The lattice constants for the lowest energy $(3_h \times 1 \times 1)$ generated structures are reported in Table 3. Although, given the larger cell, the lattice parameters and cell volume are different to those of the $(1 \times 1 \times 1)$ cell, comparison can be made by dividing the $(3_h \times 1 \times 1)$ cell volume and lattice energy by three but for the *a* and *b* parameters by $1/\sqrt{3}$. The *c* axis remains is the same. It is interesting to note that the predicted lattice parameters for the $(3_h \times 1 \times 1)$ cell are all in particularly good agreement with the experimental data. Whilst this may seem encouraging, there are many configurations with similar energies (as illustrated in Fig. 5) so that a configurational average needs to be used. Here we consider configurationally averaged temperatures of 300 K and 1000 K. Disappointingly these predicted lattice properties (see Table 3) are identical to the configurational average derived from the $(1 \times 1 \times 1)$ configurations. In fact, the majority of $(3_h \times 1 \times 1)$ configurations do not appear in the configurational average at 1000 K (see insert in Fig. 5), therefore, the configurational average is distinct from the mean. Nevertheless, it does consist of a significant number of configurations and could explain why the previous assumption of an average was useful in describing the experimental data.

2.3. Model predictions

Given that the different models examined here (see Table 3) cannot be resolved through comparison of lattice parameters, we next generate diffraction patterns in order to investigate if these might offer a mechanism for differentiation. Specifically we wish to discover if the different models give rise to additional or missing reflections or significantly different peak intensities. A simulated XRD pattern was produced from the final model refined by Yashima et al. [11] and is displayed in Fig. 7 (designated Yashima et al. model). This is compared to a spectra simulated on the basis of the lowest energy configuration derived using the $(3_h \times 1 \times 1)$ unit cell, the lowest energy configuration for the $(1 \times 1 \times 1)$ unit cell and the $(3_h \times 1 \times 1)$ supercell configurationally averaged structure. To make the identification of differences in peak absences or interstitials clear, the a and c lattice parameters for each structure were fixed as 10.4352 Å and 37.4029 Å, respectively, matching those of the experimentally determined structure [11]. Thus, our intention here is to discover if the different configurations and models give rise to sufficient differences in reflections that they may be differentiated by comparison to subsequent high resolution diffraction experiments. (Note: we also generated patterns based on neutron diffraction and these give rise to identical conclusions to those given below.)

Fig. 7 shows that all simulation models share a very similar spectra to the XRD pattern simulated from Yashima's experimental model [11]. The change in intensity of the peak at 22.4 2θ is due to the change in Ca(4) site ordering across the structure. For example, the experimental Yashima [11] model has been ascribed a Ca(4) occupancy of 0.43 and when spectra from this, and a

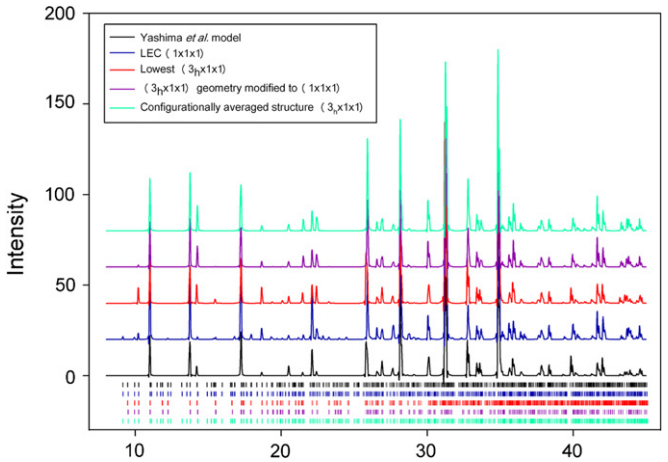

Fig. 7. Simulated XRD patterns for the experimentally derived model [11], the lowest energy configuration for both the $(1 \times 1 \times 1)$ and $(3_h \times 1 \times 1)$ cells and the geometrically modified lowest $(3_h \times 1 \times 1)$. ($\lambda = 1.54$ Å).

model with 0.5 occupancy (in order to maintain a $Ca_3(PO_4)_2$ stoichiometry), are compared there is no perceptible difference in peaks. However, when the structure is ordered (with 3 fully occupied and 3 unoccupied sites), the peak intensities at 22.4 2θ appear slightly different, Fig. 7. Conversely, the LEC $(1\times1\times1)$ exhibits some additional peaks due to the change in symmetry from *R* 3*c*, seen in the mean field experiment to, *R* 3.

As an alternative to configurational averaging, the $(3_h\times1\times1)$ cell was mapped back to the $(1\times1\times1)$ unit cell geometry, generating a new partial occupancy on the Ca(4) sites, enabling better comparison between the experimental and simulated models. This change in geometry gives rise to a new partial occupancy of the Ca(4) site. Yashima et al. originally specified an occupancy of 0.43 on each Ca(4) which, using the modified geometry cell, changes to an occupancy of either a $\frac{1}{3}$ or $\frac{2}{3}$ in an alternating configuration. This modified $(3_h\times1\times1)$ cell also exhibits a similar XRD pattern with some differences in intensity and observed reflections to those found in the spectra simulated from the data of Yashima et al.; these differences can be attributed to Ca(4) site occupancy. As expected the mean field data also shares a comparable XRD spectra to this larger cell size.

3. Conclusions

A classical pair potential model has been used to generate a number of possible structures for β−$Ca_3(PO_4)_2$. The challenge in describing this structure comes from the half occupation of a Ca 6*a* site, Ca(4), which leads to a large number of potential configurations. We have investigated all possible configurations in a single $(1\times1\times1)$ unit cell and identified the most stable variant. Furthermore, all configurations were computed for a hexagonal symmetry $(3_h\times1\times1)$ cell and significantly lower energy configurations were found. These latter model configurations exhibit $P3_1$ and $P3_2$ symmetries, isomorphic supergroups of the unit cell symmetry *R* 3*c*, which is the experimentally determined structure [11]. However, given the small energy differences between a large number of low energy $(3_h\times1\times1)$ configurations, the experimental structure will not reflect just one specific order of Ca ions over Ca(4) sites. This helps justify the previous assumption of an average occupancy.

The $(3_h\times1\times1)$ cell was chosen for larger simulations because it exhibits the full symmetry of the experimentally determined space group. Nevertheless, we have not been able to discount the possibility that an even larger cell would offer a single order that is even more stable, thought, of course, configurational entropy will be acting against this. It is clear, however, particularly from the $(1\times1\times1)$ results that simulations must include lattice relaxation if useful energies and structures are to be generated. This makes multiple simulations of cells larger than $(3_h\times1\times1)$ a formidable task.

The questions raised at the start of this paper were: is the Yashima partial occupancy model valid on an atomic scale and if so, what is the nature of the disorder? We have certainly found that, given the low symmetry of the β−$Ca_3(PO_4)_2$ structure, the Yashima et al. [11] model is a reasonable description. We have found for example, no evidence of any disorder on the Ca(5) site, in agreement with the model description. It has been shown, however, that there are differences in the stability of the structures when we consider specific ordered configurations, both within the original primitive cell and in larger supercell structures. The observed partial occupancy is not random: the probability of finding a Ca atom on a given site does depend upon the occupancy of local sites at least in a $(1\times1\times1)$ cell. Using the LEC for a $(3_h\times1\times1)$ cell and modifying the geometry to compare to experiment, we find that a more suitable representation of the half occupancy is for the Ca(4) sites to be occupied down the c axis in a $\frac{1}{3}$, $\frac{2}{3}$ repeating pattern instead of all being half occupied.

Crucially, however, when we examine a larger hexagonal supercell of the primitive unit cell we have found many different configurations with similar energies and with distinct cation arrangements that are substantially more stable that the most stable configuration of the primitive unit cell. We are unable to identify a single low energy cell or structural motif that will dominate in a real crystal. In fact, we propose that the structure could consist of numerous small domains formed during materials synthesis each with distinct cation ordering of one of the lower energy supercell configurations, but lacking the thermodynamic driving force to adopt a single, ordered crystal. In a diffraction experiment, which by its very nature, samples the order of a material over long ranges, the observed spectrum will be a superposition of many of these domains. Thus, on average the cation sites will appear disordered. Nevertheless, the order in these domains, even on a sub-grain level will be of crucial importance in determining the behaviour of extrinsic dopants and contributes to the compositional flexibility of the tricalcium phosphate systems. In this regard, the lowest energy $(3_h\times1\times1)$ structure identified here is a useful model on which to base such investigations.

Acknowledgments

EMM and EEJ acknowledge AWE for financial support. This work was party carried out as part of the TSEC programme KNOO and as such we are grateful to the EPSRC for funding under Grant EP/C549465/1. Computing resources were provided by the Imperial College High Performance Computing Service (http://www.imperial.ac.uk/ict/services/teaching-andresearchservices/highperformancecomputing). British Crown Owned Copyright 2010/MOD.

References

[1] B.L. Jolliff, J.M. Hughes, J.J. Freeman, R.A. Zeigler, Am. Miner. 91 (2006) 1583–1595.
[2] A. Legrouri, S.S. Romdhane, J. Lenzi, M. Lenzi, G. Bonel, J. Mater. Sci. 31 (1996) 2469–2473.
[3] H.D. Foth, B.G. Ellis, Soil Fertility, Environmental Science Agriculture and Soils, Lewis Publishers, USA, 1997, p. 154.
[4] L. Hench, J. Wilson, An Introduction to Bioceramics, World Scientific, 1993.
[5] A.I. Orlova, Radiochemistry 48 (2006) 561 1066-3622.
[6] A.I. Orlova, Crystallograph. Rept. 50 (2005) 48–51 1063-7745.
[7] A.I. Orlova, Radiochemistry 48 (2006) 330–339.
[8] F. Goetz-Neunhoeffer, J. Neubauer, R. Enderle, M. Gobbels, Zeitschr. Kristallograph. (2007) 375–380.
[9] M. Mathew, L.W. Schroeder, B. Dickens, W.E. Brown, Acta Crystallogr. B 33 (1977) 1325–1333.
[10] B. Dickens, J. Solid State Chem. 10 (1974) 232–248.
[11] M. Yashima, A. Sakai, T. Kamiyama, A. Hoshikawa, J. Solid State Chem. 175 (2003) 272–277.
[12] B.I. Lazoryak, V.A. Morozov, A.A. Belik, S.S. Khasanov, V.S. Shekhtman, J. Solid State Chem. 122 (1996) 15–21.
[13] K. Yoshida, H. Hyuga, N. Kondo, H. Kita, J. Am. Ceram. Soc. 89 (2006) 688–690.
[14] R. Gopal, C. Calvo, Nat. Phys. Sci. 237 (1972) 30–32.
[15] J.D. Gale, J. Chem. Soc. Faraday Trans. 93 (1997) 629–637.
[16] J. Nocedal, S.J. Wright, Numerical Optimization, Springer Series in Operations Research, Springer-Verlag, 1999.
[17] P. Ewald, Ann. Phys. 369 (1921) 253–287.
[18] D. Mkhonto, N.H. de Leeuw, J. Mater. Chem. 12 (2002) 2633–2642.
[19] I.T. Todorov, N.L. Allan, M.Y. Lavrentiev, C.L. Freeman, M.C.E., J.A. Purton, J. Phys.: Condens. Matter 16 (2004) S2751 0953-8984.
[20] N.J. Ashley, R. Grimes, K. McClellan, J. Mater. Sci. 42 (2007) 1884–1889.
[21] X. Yin, M.J. Stott, A. Rubio, Phys. Rev. B 68 (2003) 205205–205213.